Journal of Universal Computer Science, vol. 32, no. 10 (2026), 1492-1520
submitted: 7/9/2025, accepted: 19/1/2026, appeared: 28/9/2026 CC BY 4.0

Energy Prediction Based on Periodic Mechanical Impact in PVDF-Based Piezoelectric Energy Harvesting: A Comparative Analysis of Machine Learning Models

Sertac Kaan Tokyay
(Aksaray University, Aksaray, Turkey
https://orcid.org/ 0000-0003-0762-939X, skaantokyay@gmail.com)

Hasan Demir
(Aksaray University, Aksaray, Turkey
https://orcid.org/ 0000-0001-5424-7242, hasandemir@aksaray.edu.tr)

Atıl Emre Cosgun
(Aksaray University, Aksaray, Turkey
https://orcid.org/ 0000-0002-4889-300X, atilemrecosgun@aksaray.edu.tr)

Abstract: In this study, an experimental setup was established to measure the energy that can be harvested depending on the frequency of periodic mechanical pulses using Polyvinylidene Fluoride (PVDF) piezoelectric material. The measured data were employed in Artificial Neural Network (ANN), K-Nearest Neighbours (KNN), Support Vector Machine (SVM), and Random Forest (RF) algorithms, and the models were compared in terms of prediction performance and processing time. The performance of the models was evaluated using regression success metrics such as coefficient of determination (R^2), root mean square error (RMSE), mean absolute error (MAE), Nash-Sutcliffe Efficiency (NSE), computation time and additionally Taylor diagram and Bland-Altman analysis were applied to further evaluate the accuracy and reliability of the models. According to the results, all models achieved high accuracy, with the highest R^2 value obtained from the RF model (R^2 = 0.9756), followed closely by SVM (R^2 = 0.9752) and ANN (R^2 = 0.9730). The RF model also showed the lowest error rates (MAE = 3.5874, RMSE = 8.7020) and a strong NSE value (0.9751), making it the most balanced and reliable model overall. The ANN model demonstrated competitive performance, though a noticeable gap was observed between training and testing errors (MSEtrain = 139.76 vs. MSEtest = 86.59), indicating potential overfitting tendencies. The KNN model, despite its very fast computation time (0.0066 s), exhibited lower predictive accuracy compared to the other models (R^2 = 0.9464, RMSE = 16.6871). These findings suggest that Random Forest provides the best compromise between accuracy, stability, and efficiency for piezoelectric energy harvesting prediction tasks. The developed predictive models will serve as a valuable reference for researchers conducting feasibility studies, particularly in applications such as powering CMOS circuits and sensors through periodic pulse-based energy harvesting.

Keywords: Piezoelectric Energy Harvesting, Artificial Neural Network (ANN), K-Nearest Neighbour (KNN), Support Vector Machine (SVM), Random Forest (RF)
Categories: H.3.1, H.3.2, H.3.3, H.3.7, H.5.1
DOI: 10.3897/jucs.171383

1 Introduction

Nowadays, energy efficiency and sustainability issues have become increasingly critical, especially with the rise of portable electronic devices and IoT systems. The significant reductions in power consumption of sensors and CMOS circuits have increased research into embedded power sources [Tarun et al., 2015, Sung et al., 2019, Mahyar et al., 2019, Faizan et al., 2019, Huicong et al., 2018]. Sensors in distributed areas, structural health monitoring sensors in remote locations, data collection components, and sensors in geographically inaccessible areas become impractical due to issues such as battery charging or replacement [Shashank et al., 2019, Mikko et al., 2016, Jie et al., 2018, Henry et al., 2004, Shima et al., 2018]. In large-scale sensor networks located in areas such as urban areas, the costs of charging or replacing batteries reach significant levels [Priya et al., 2009]. In line with these needs, piezoelectric energy harvesting (PEH) systems that convert vibrational energy into electrical energy have gained significant importance. Especially cantilever, bimorph, and unimorph structured piezoelectric chips offer effective energy conversion in both micro-scale and macro systems [Shashank et al., 2019].

Piezoelectric materials can be used in different ways such as vibration, bending (cantilever), compression, and impact, depending on the type of mechanical stress applied to them [Chengyun et al., 2021, Domenico et al., 2022, Harvey et al., 2022, Bin et al., 2022]. Among these, the most common type of application is piezo patches placed on cantilever structures. In cantilever structures, mechanical stress is generally generated by periodically striking the piezoelectric material. These structures, while providing an advantage in harvesting energy from low-frequency vibrations, require multi-modal or non-linear solutions due to operational limitations at resonance frequencies [Yuzhong et al., 2020]. Due to their simple structures and significant deformation during vibration, cantilever beam structures are a major preference in PEH. Therefore, different cantilever beam structures have been used to improve the harvested power output [Shima et al., 2018, Yuzhong et al., 2020, Cevat et al., 2021, Hao et al., 2013, Linbing et al., 2019, Baozhi et al., 2021].

The determination of the power output of piezoelectric materials based on mechanical stress facilitates the prediction of results for many applications. Especially multimodal behaviours, environmental noise, and mechanical uncertainties make it difficult to predict power output. Therefore, various prediction algorithms such as ANN, KNN, SVM, and RF are developing models trained with data. These algorithms achieve significant success due to their high modelling capacity in nonlinear multivariate systems.

While the use of machine learning models in PEH is becoming increasingly widespread, advanced approaches focused on improving resource management and prediction capabilities in more complex and dynamic systems are gaining prominence in the literature. Deep Reinforcement Learning (DRL) and Multi-Agent Deep Learning (MADL) architectures play a critical role in overcoming the limitations of static configurations and traditional management methods, particularly in environments with dynamic and variable traffic patterns such as Mobile Edge Computing (MEC) and Mobile Ad-Hoc Networks (MANETs) [Shuhong et al., 2024, Amin et al., 2025]. These frameworks optimize adaptive resource slicing (network slicing) and computational offloading decisions to ensure compliance with Service Level Agreement (SLA)

constraints and maximize throughput. For example, in MEC networks, specialized mechanisms such as the Sparse Multi-Head Graph Attention Mechanism (SMHGA) are used to increase the accuracy of traffic prediction and capture complex spatiotemporal dependencies. These predictions are combined with advanced DRL algorithms such as Twin Delayed Deep Deterministic Policy Gradient (TD3). Furthermore, in heterogeneous cellular networks where unmanned aerial vehicles (UAVs) are enabled, Graph Neural Networks (GNNs) are used to dynamically adapt resource allocation decisions based on the network topology [Qinghua et al., 2025]. Technologies such as Smart Reflective Surfaces (IRS) and Serverless Federated Learning (FL) are integrated with MADL approaches to optimize energy efficiency and coverage. These methods offer the potential to manage large-scale, continuous data streams to understand the dynamics of environmental systems such as energy harvesting and to enhance real-time prediction capabilities, demonstrating a level of real-time adaptation and optimization beyond traditional Machine Learning models.

Recently, various machine learning algorithms have been successfully employed in different engineering prediction problems, demonstrating their strong capability in modelling nonlinear systems. Artificial Neural Networks (ANN) have shown high performance in complex pattern recognition tasks such as sign language recognition and dynamic system modelling [Irvanizam et al., 2023]. Support Vector Regression (SVR) has been effectively applied for accurate regression in chemical and industrial process prediction problems, including the prediction of Kovats retention indices in gas chromatography [Teuku et al., 2022].

Moreover, hybrid optimization and machine learning approaches have been adopted for electrical and energy-based systems, as reported in recent IEEE studies [Aga et al., 2020, Mariza et al., 2022], where ANN and SVM-based models achieved high prediction accuracy under nonlinear operating conditions. These studies indicate that ANN, KNN, SVM, and RF are not only computationally efficient but also highly reliable for small-to-medium experimental datasets.

ANN are frequently preferred for prediction due to their deep layered structure, high learning capacity, and ability to model nonlinear system behaviours [Prabina et al., 2016, Umit et al., 2021, Priyadarshini et al., 2017]. However, the RF algorithm also offers a combination of high accuracy and low variance thanks to the ensemble learning approach; it demonstrates strong generalization ability even with limited samples [Chengyun et al., 2021, Thomas, 2000, Leo, 1996, Robert et al., 2007]. The RF algorithm is faster, more interpretable, and resistant to overfitting [Wael et al., 2022, Jaime et al., 2019]. On the other hand, SVM stands out for its ability to provide high performance, especially with small datasets, and its capability to separate complex structures using kernel functions [Serkan and Burcu, 2024, Bishal et al., 2024].

Finally, the KNN algorithm provides the advantage of rapid prototyping in low-complexity systems because it is based on the principle of direct distance measurement without the need for parameter tuning. This method is particularly preferred in small datasets and real-time applications. However, as the data sizes increase, there is a slowdown [Ernest et al., 2020, Ismail et al., 2008].

This research aims to create a predictive model for the power output of flexible Polyvinylidene Fluoride (PVDF) piezoelectric material, influenced by impact frequency, utilizing ANN, KNN, SVM, and RF algorithms. Comparisons of accuracy and performance among several prediction algorithms have been conducted. The assessment of the models' predictive ability included criteria including the R^2, RMSE,

MAE, and NSE. In addition to classical error metrics, Taylor diagrams and Bland-Altman analysis were applied to thoroughly evaluate the accuracy and reliability of the developed models. The study's findings will aid in forecasting the strength of PVDF materials under periodic impact stress.

The remainder of this paper is organized as follows. Section 2 describes the experimental setup and the physical modelling of the impact-driven PVDF-based piezoelectric energy harvesting system. Section 3 presents the data pre-processing procedures and the implemented machine learning methodologies. Section 4 discusses the results of the comparative performance analysis using statistical and graphical evaluation tools. Finally, Section 5 concludes the paper and outlines future research directions.

2 Theoretical Modelling of Piezoelectric Harvester

The piezoelectric energy harvesting system used in this study consists of a PVDF piezoelectric film layer bonded to a cantilever beam subjected to periodic pulse excitation. The conversion of mechanical energy into electrical energy begins with the displacement at the tip of the cantilever, continues with electrical displacement and charge generation on the piezoelectric layer thru normal strain caused by bending. Under the impact of the blow, the cantilever beam primarily oscillates in its first vibration mode, and its fundamental natural frequency is expressed by Equation 1.

$$f_1 = \frac{1.875^2}{2\pi L^2}\sqrt{\frac{EI}{\rho A}} \tag{1}$$

Where L represents the beam length, E is the modulus of elasticity, I is the second moment of area, ρ is the density, and A is the cross-sectional area. The impact-induced vibration produces the displacement at the end of the beam, which results in a bending moment along the beam and normal stress on the PVDF layer. The mechanical energy-electrical energy conversion chain is fundamentally determined by the normal strain ε resulting from bending.

In piezoelectric materials, mechanical strain leads to electrical displacement and the creation of electric charge. The piezoelectric constitutive equation for PVDF can be represented as given in Equation 2.

$$\mathrm{D} = d_{31}\sigma + \varepsilon^T E \tag{2}$$

In this analysis, the electric field term was disregarded, and the resultant surface electrical displacement was considered to be predominantly attributable to mechanical stress. Accordingly, the resulting electric charge is given by Equation 3.

$$\mathrm{Q} = d_{31}\sigma A \tag{3}$$

Where, D represents the electric displacement, d_{31} is the piezoelectric coefficient of the PVDF material, σ is the normal mechanical stress due to bending, and A is the

electrode area. This statement indicates that mechanical strain is directly converted into the production of electrical charge.

The electrical charge generated on the PVDF layer transforms into open-circuit voltage under open-circuit conditions, and this voltage is expressed by Equation 4.

$$V_{oc} = \frac{Q}{C_p} \tag{4}$$

Here, V_{oc} is the open-circuit voltage, Q represents the generated electric charge and C_p represents the electrical capacitance of the PVDF layer. Thus, a sequential energy conversion chain emerges: extreme displacement → bending → normal strain → electrical displacement → electric charge → open-circuit voltage.

There are fundamental parameters that affect the conversion of mechanical energy into electrical energy and energy production. In this study, the cantilever beam structure shown in the cross-sectional geometry in Figure 1 can be summarized as follows: beam length 20 mm, PVDF layer thickness 28 μm, tip displacement 17.4 mm, and load resistance 20K Ohm.

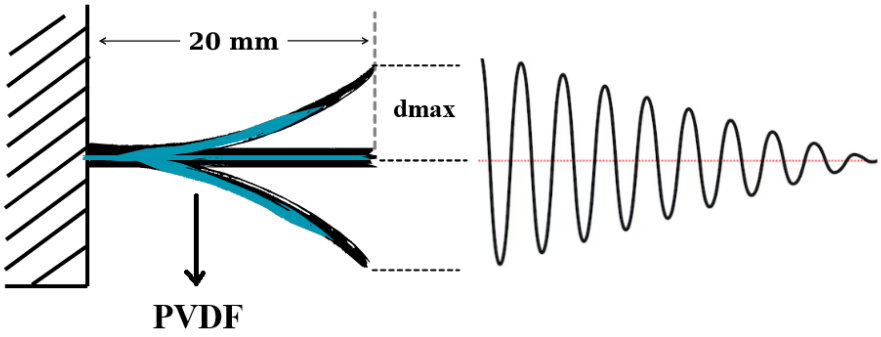

Figure 1: Schematic diagram of console-type energy harvesting created using PVDF

For transparency and reproducibility, we summarize the key geometrical and electrical parameters used to evaluate the governing relations of the PVDF harvester in Table 1.

Active sensor area	A = 20 x 9 mm^2 = 1.8 x 10^{-4} m^2
Film thickness	28μm
Specified typical capacitance	$C_p \approx 500$ pF
Piezoelectric coefficient	d_{31} = 10 pC/N
Bending-induced normal stress	σ = 1.0 x 10^6 (Pa)

Table 1: Geometrical and electrical parameters of the PVDF [Measurement Specialties, 1999]

The piezoelectric effect and capacitance relationship, along with the transformation chain, can be found using Equations 3 and 4. Based on the parameters in Table 1, the electric charge Q = 1.8 x 10^{-9} C and the open-circuit voltage (V_{oc}) were calculated to be approximately 3.6 V. Experimental uncertainties arise primarily from sensor resolution and pulse repeatability, and an error of approximately 4.38% was calculated for the open-circuit voltage. These order estimates are consistent with the experimental open-circuit voltage measurements in our study. Furthermore, the governing equations are not intended for direct analytical prediction of harvested energy but rather to provide physical consistency for the experimental dataset used in machine learning training.

A parametric sensitivity analysis indicates that an increase in beam length and elastic modulus leads to higher strain-induced charge levels, whereas variations in the dielectric constant primarily affect the voltage amplitude. These trends are consistent with both theoretical expectations and experimental observations.

This theoretical framework reveals that the dataset used in the study is based not only on experimental measurements but also on well-defined laws of mechanical-electrical energy conversion, forming the physical basis of the machine learning-based prediction approach.

3 Experimental setting and data collection

3.1 Design concept

Piezoelectric materials are substances that generate opposite charges at both ends under mechanical stress and produce a weak voltage. Piezoelectric materials, which can be produced in different shapes and material structures, generate different voltage values depending on the magnitude of the mechanical strain and the frequency of application. Polyvinylidene Fluoride is a common polymer that exhibits piezoelectric properties with high flexibility. It is generally preferred in low-frequency vibration energy harvesting applications. The piezoelectric coefficient is low; therefore, it generates low voltage, but it provides an advantage with its light weight and workability. Console-type PEH applications are frequently used.

In this study, a cantilever-type energy harvesting experimental setup created using PVDF piezoelectric material has been proposed. To simulate mechanical stress, a wheel mechanism designed in a computer environment and produced with a 3D printer was mounted on a stepper motor. The rotational speed of the step motor was both measured and controlled, and the number of impacts per minute, or impact frequency, of the PVDF piezoelectric material subjected to periodic mechanical impact stress was calculated. The output power obtained from PEH will be measured based on the impact frequency. The measured output power will be used to develop a prediction model by training ANN, RF, SVM, and KNN prediction algorithms.

3.2 Experimental setting

In Figure 2a and 2b, the cantilever-type energy harvesting experimental setup is constructed with PVDF piezoelectric material (LDT0-028K). The technical specifications of PVDF are provided in Table 2. Mechanical vibration is generated with a wheel and pin produced by a 3D printer mounted on the stepper motor shaft. The

rotation speed of the wheel is controlled by the stepper motor driver (TB6600) and measured with the LM393 Sensor Module. The speed measured in revolutions per minute is converted to the multiplication frequency with Equation 5.

$$Frequency\ (Hz) = \frac{Number\ of\ Impacts\ (unit: counts/min)}{60} \tag{5}$$

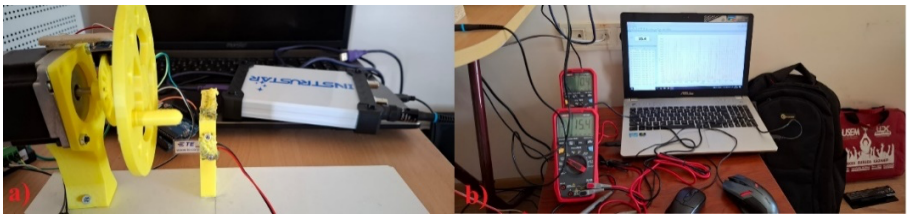

Figure 2: Console-type energy harvesting experimental setup created using PVDF; a) PVDF piezoelectric material and b) measuring instruments

Material	28µm Piezoelectric Film
Sensitivity	High Sensitivity AC Coupling
Design	Cantilever Beam Structure
Operating Temperature	0 ~ 85°C
Storage Temperature	-40 ~ 85°C

Table 2: Technical specifications of the PVDF piezoelectric material (LDT0-028K)

After the impact frequency is measured, the voltage signal produced by the PVDF piezoelectric transducer is measured and recorded by a digital oscilloscope (ISDS205B). The voltage signal is commonly converted to DC voltage using a DC-DC buck circuit. The LTC-3588 chip, marketed by Linear Technology, is utilized in PEH systems and incorporates a full-wave rectifier along with a high-efficiency DC-DC buck converter. The power of the electrical energy extracted from the LTC-3588 circuit is calculated with a 20 K Ohm load resistor. To understand the energy harvesting process, Figure 3 shows the general schematic of the system where the energy produced by the PVDF piezoelectric transducer is converted using the LTC-3588 circuit.

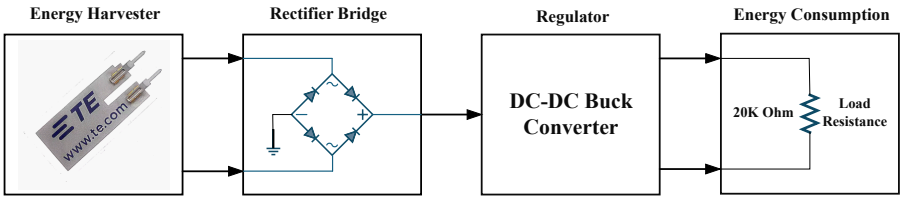

Figure 3: The general schematic of the PVDF PEH system

PVDF materials are used in cantilever-type energy harvesting structures because they are very thin and flexible. The piezoelectric open-circuit voltage given in Equation 4 was explicitly shown in Equation 6 when examined using energy management by Sun and colleagues [Chengliang et al., 2009].

$$V_{oc} = \frac{Q}{C_p} = \frac{F_0 E_p t_p d_{31}(t_p + 2a)L}{w t_p d_{31}^2 E_p^2 (t_p + 2a)^2 + 4EI(\varepsilon_{33}^T - E_p d_{31}^2)} \tag{6}$$

Where Ep is the young's modulus of the piezoelectric layer in the length direction, L is the equivalent length of the beam, d_{31} is the piezoelectric constant in 31 mode, t_p thickness of the piezoelectric layer, EI is the flexural rigidity of the beam, ε^T_{33} is the permittivity of the piezoelectric at constant stress. F_0 represents the static force applied at the free end, resulting in a deflection of $F_{0/k}$.

The output voltage of the LTC-3588 circuit is fixed at 3.6 V. The energy harvesting system's ability to continuously convert the collected energy into usable power is achieved with a 20 K Ohm load resistance, and the current and voltage measurements are shown in Figure 2b. In Figure 4, the electrical schematic of the energy harvesting system is shown.

Voltage output signals were obtained under controlled laboratory conditions at room temperature and humidity. Different pulse excitation frequencies were applied to capture the dynamic behaviour of the piezoelectric response over a wide range of study. During the experiments, ambient vibration noise was minimized by isolating it from external mechanical influences, and temperature changes were kept within a narrow laboratory range to limit thermal effects on the piezoelectric output.

The impact frequency of the energy harvesting system is measured and recorded based on the current and voltage outputs and the rotation speed of the wheel. The recorded data is used to develop models using four prediction algorithms, which are the main statistical tools: ANN, KNN, SVM, and RF. To develop a reliable and accurate prediction model, the focus is on the collision frequency and harvested DC power, which are dependent on periodic mechanical stress. The flowchart in Figure 5 shows the sequential steps of developing the prediction model from the initial data collection phase to the final prediction outputs. In order to develop the models, it is necessary to take the average of the harvested power outputs. Separate prediction models have been developed for each algorithm, and their effectiveness and accuracy have been analysed through comparison. The determination of the most reliable model among the algorithms was ensured through this analysis.

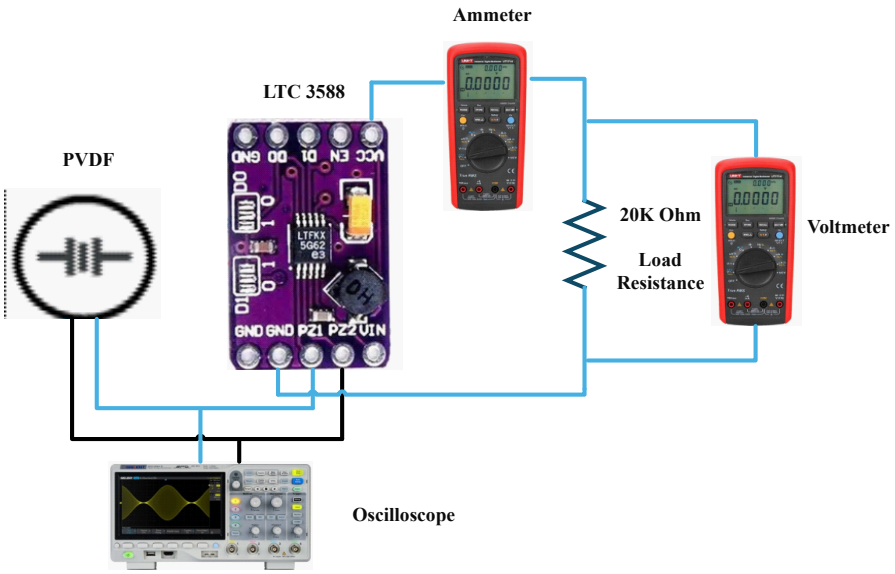

Figure 4: Electrical diagram of the PEH system

3.3 Artificial Neural Network

ANN is a machine learning algorithm based on statistical modelling that can adapt to changes based on internal and external information during the training phase, defining nonlinear complex relationships between outputs and inputs [Ahmad and Allar, 2011, Kurt et al., 1990]. ANN is generally a multilayer feedforward perceptron consisting of interconnected input, numerous hidden, and output layers. In the hidden layers and output layers, various activation functions and different types of algorithms for model training are available. A simple representation of the feedforward ANN architecture is provided in Figure 6.

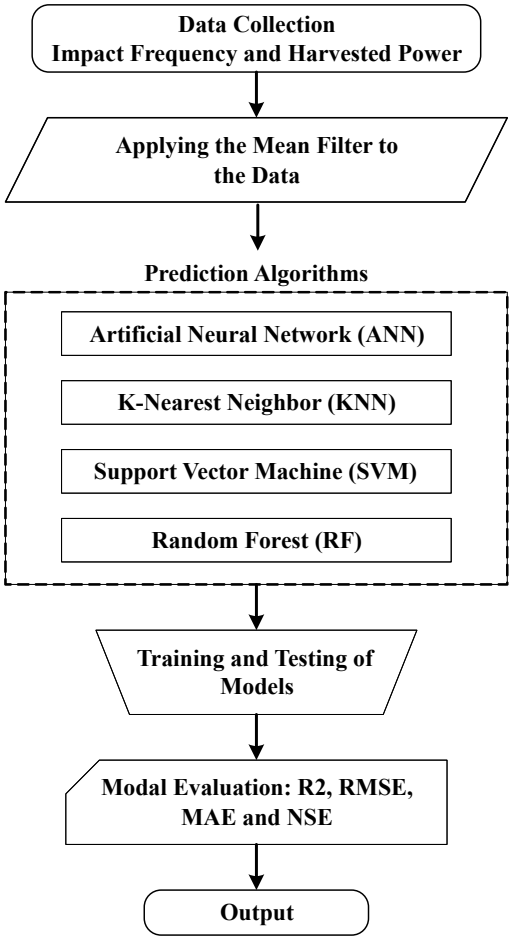

Figure 5: Flowchart showing the modelling approach used in current algorithms

This study developed an ANN model configured as a single hidden layer feedforward network. The ANN model was trained using 1058 samples and was designed with a single input and a single output neuron to match the one-dimensional structure of the dataset (1 input, 1 output). The data was partitioned into two segments: 80% allocated for model training and 20% designated for model testing. The number of neurons in the hidden layer was not arbitrarily chosen; prediction errors were compared by scanning between 3 and 20. The hidden layer had 10 neurons, with the Hyperbolic Tangent Sigmoid Function (tansig) as the activation function, as specified in Equation 7. The ten-hidden neuron network structure that yielded the lowest validation error (RMSE) was determined as the optimal architecture. In the output layer, the Linear Transfer Function (purelin), which is a linear activation function, as given in Equation 8, was preferred. The Levenberg-Marquardt (trainlm) algorithm, known for its rapid convergence, was used for training the model. The Levenberg-Marquardt algorithm

strikes a balance between Newton's method and gradient descent, and its mathematical representation is given in Equation 9. Input and output data have been normalized to the range [0, 1] using the mapminmax function. These choices ensure a balance between model complexity and generalization ability, preventing overfitting and underfitting.

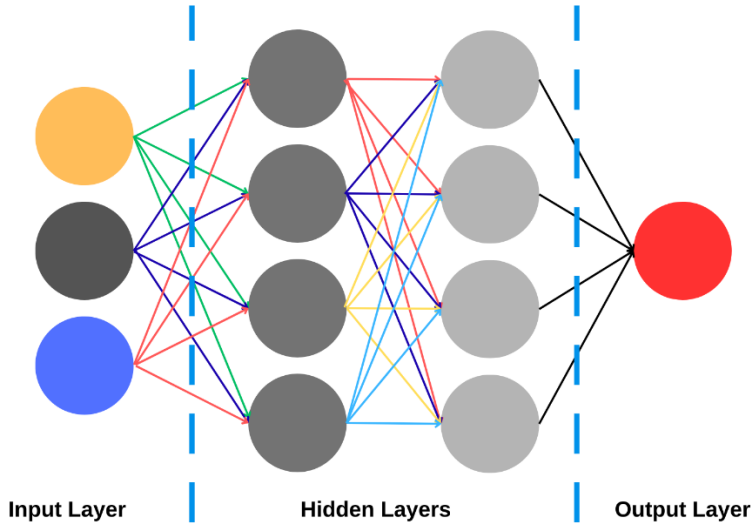

Figure 6: A simple representation of a feedforward ANN architecture

$$f(x) = \tanh(x) = \frac{2}{1 + e^{-2x}} - 1 \tag{7}$$

$$f(x) = x \tag{8}$$

$$\Delta\omega = -(J^T J + \mu I)^{-1} J^T e \tag{9}$$

In Equation 9, J is the Jacobian matrix (the network's error derivative), μ is the damping parameter, I is the identity matrix, and e is the error vector.

3.4 K-Nearest Neighbour (KNN)

KNN is a sample-based learning method that classifies based on training examples. A feature vector is determined by the majority vote of the classes of its k-nearest neighbours. To find the nearest neighbour, Euclidean distance metrics are used in the KNN algorithm. The Euclidean distance metric is given in Equation 10. When given X, KNN predicts the conditional distribution of Y and assigns a specific observation to the class with the highest predicted probability. When a positive number K is given, the algorithm identifies the K points closest to the test observation (x0) and estimates the conditional probability for the class based on the ratio of the response values [Ismail et al., 2008, Fei et al., 2004]. The KNN algorithm can be successful with noisy data and a

large number of training samples. For this algorithm, it is sufficient to determine the k parameter and the type of distance to be used, and there is no need to create a model, adjust a few parameters, or make additional assumptions.

$$d(x,y) = \sum_{i=1}^{N} \sqrt{x_i^2 - y_i^2} \tag{10}$$

Where, N is the number of features.

In the KNN model of this study, for each test sample, the 5 nearest neighbours from the training data were selected, and the average of these neighbours' target values was taken to make the prediction. The k value was scanned within the range of 1–15, and prediction errors were calculated for each value. Because the lowest error was obtained at k = 5, the final model was created with this value. Due to the continuous nature of the input variable and the low-dimensionality of the dataset (one input – one output), Euclidean distance was used as the distance metric. This optimization process increases the reliability of KNN-based predictions and allows for fair comparison with other machine learning models. This algorithm stands out for not requiring a training process and making direct predictions.

3.5 Support Vector Machine

SVM is a model of supervised learning that employs associated algorithms for data regression analysis and classification. The data is divided into two or more classes to create a dataset. A kernel function, which is a mapping procedure applied to the training set to increase the dimensionality of the data set, is used. Linear, RBF, second-degree, Multi-Layer Perceptron kernel, and Polynomial kernel are some of the commonly used kernel functions [Corinna and Vladimir, 1995]. In the case where the problem is not linearly separable, it would be appropriate to use an SVM with a non-linear kernel such as the Radial Basis Function (RBF) [Suykens and Vandewalle, 1999]. In Equation 11, the mathematical expression of the RBF is given. Figure 7 shows a simple SVM topology.

$$K(x_i, x_j) = \exp(-\gamma \parallel x_i - x_j \parallel^2) \tag{11}$$

Where K (x_i, x_j) is the similarity between the data points x_i and x_j, $\|x_i - x_j\|^2$ is the square of the Euclidean distance between two points, and γ is the kernel width (degree of freedom parameter).

In this study, the support vector machine (SVM) model was configured using the Gaussian radial basis function (RBF) kernel for regression purposes due to its strong capability to model non-linear relationships between mechanical excitation and electrical output in piezoelectric energy harvesting systems. The RBF kernel maps the input data into a high-dimensional feature space, enabling accurate representation of complex system dynamics that cannot be captured by linear models. Given that the dataset consists of a limited number of samples (1058 data points with one input and one target), SVM was particularly suitable because of its robust generalization performance in small-sample scenarios. The kernel and regularization parameters were selected through parametric tuning to minimize the validation error, providing

improved noise immunity and stable prediction performance under low-frequency impact excitation.

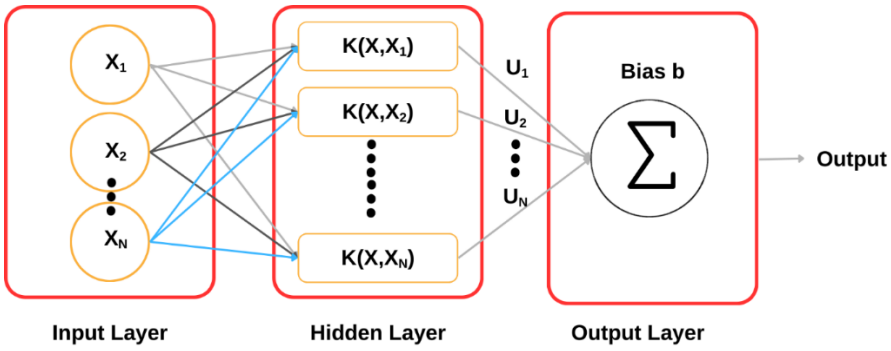

Figure 7: A simple general representation of the SVM topology

3.6 Random Forest

RF variances are effectively managed through the aggregation of decision trees. It is used in both regression and classification tasks. Probabilistic binary trees are created in the RF regression model using subsets of observations obtained through bootstrapping. To contribute to the development of the model, the process of bootstrapping is used, where a portion of the training data is randomly sampled from the dataset. RF models are a type of ensemble model that generates predictions using a combination of base models. This class of models is mathematically expressed as the sum of individual base models, where each base model is a decision tree, as shown in Equation 12 [Jaime et al., 2019]. A general visual representation of this approach, explained as model ensemble, is provided in Figure 8.

$$g(x) = f0(x) + f1(x) + f2(x) + f3(x) \ldots \tag{12}$$

In this study, the RF model was implemented as an ensemble learning method consisting of 50 regression trees. Each tree was trained on a different bootstrap sample of the original dataset, while a random subset of features was considered at each split to enhance model diversity. The final prediction was obtained by averaging the outputs of all trees, which effectively reduces variance and improves generalization performance. The number of trees was selected based on a parametric analysis showing that performance gains saturated beyond 50 trees while computational cost increased. Owing to its inherent robustness against noise and overfitting, the RF model is particularly suitable for capturing the non-linear and stochastic behaviour of piezoelectric energy harvesting under periodic impact excitation.

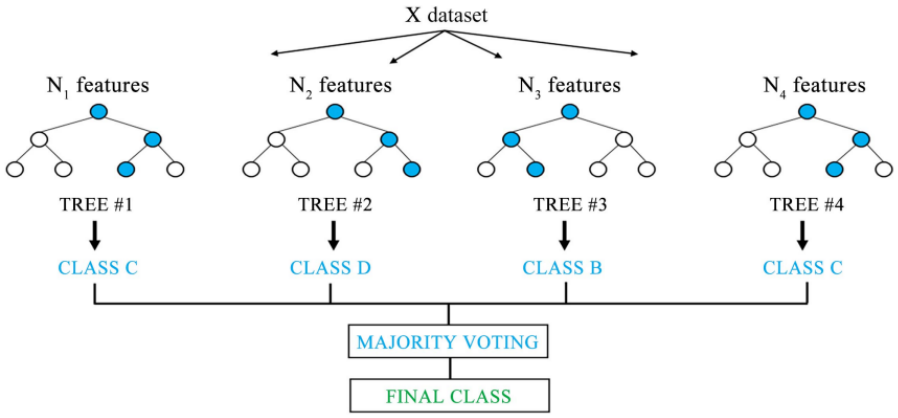

Figure 8: Random Forest regression structure [Boateng et al., 2020]

3.7 Hyperparameter Settings and Models Configuration

Table 3 summarizes the hyperparameters and implementation details of all machine learning models used in this study. The dataset consisted of 1058 samples with a single-input-single-output structure, and a hold-out validation method was used for training and testing at a rate of 80%–20%. Min–max normalization was applied to the input and output data in the ANN model. A single-layer structure with ten neurons was used in the hidden layer, with a tansig activation function in the hidden layer and a linear activation function in the output layer. Network training was performed using the Levenberg–Marquardt backpropagation algorithm for a maximum of 1000 iterations. Overfitting was also verified by comparing the training and test squared errors.

In the KNN model, the number of neighbours was set to k = 5, weighting was uniform, and absolute distance was used as the similarity metric. The SVM model was implemented for regression using a Gaussian (RBF) kernel. The regularization parameter and kernel scaling factor were determined by the internal data-driven optimization procedure of the MATLAB regression SVM solver, ensuring stable generalization performance without manual bias in parameter selection. The RF regression was constructed from 50 decision trees trained using bootstrap sampling, and variable importance was additionally assessed using OOB (out-of-bag) permutation error. This systematic documentation of hyperparameters ensures that comparisons between models are transparent, reproducible, and scientifically sound.

Model	**Hyperparameter**	**Value**	**Determination / Source**
YSA	Hidden layers	1	Compact structure to avoid overfitting

	Neurons in hidden layer	10	Selected via parametric sweep (3–20) + minimum RMSE
	Activation function	Purelin	Suitable for regression
	Training algorithm	Levenberg–Marquardt	Fast convergence and stability
	Epochs	1000	MATLAB default
	Overfitting control	Training vs test MSE	Explicitly evaluated
KNN	Number of neighbours (k)	5	Optimized in the range k = 1–15 (minimum validation error)
	Distance metric	Euclidean	Continuous low-dimensional feature space
	Weighting scheme	Uniform	Prediction stability
SVM	Kernel function	Gaussian (RBF)	Captures non-linear relationships
	Regularization (C)	Automatic (MATLAB default)	fitrsvm default
	Kernel scale (γ)	Automatic (MATLAB default)	fitrsvm default
	Loss function	ε-insensitive	Robust against noise
RF	Number of trees	50	Performance saturation observed beyond this value
	Bootstrap sampling	Enabled	Increases model diversity
	Feature selection per split	Random subset	Reduces tree correlation

Table 3: Hyperparameters of the Machine Learning Models Used in this Study

3.8 Parameters for evaluating the accuracy of prediction models

Following the development of prediction algorithms, it is imperative to assess the accuracy of the models. This study evaluates the prediction models using R^2, MAE, RMSE, and NSE efficiency indices, along with training and testing errors, and advanced statistical visualization techniques such as the Taylor Diagram and Bland–Altman analysis**.**

The R^2 number spans from 0 to 1, with elevated values signifying great precision and a minimal margin of error. The NSE ranges from $-\infty$ to 1, with a value of 1 signifying a flawlessly matched predictive model. RMSE, being the square root of the average squared prediction errors, places greater weight on large discrepancies, hence lower RMSE values indicate superior model performance. MAE represents the average absolute deviation between predicted and actual values; smaller values signify more accurate models.

In addition, training and testing errors were computed separately to evaluate potential overfitting or underfitting tendencies. A noticeable discrepancy between training and testing errors implies reduced generalization ability, whereas similar values suggest a well-balanced model.

Beyond classical error metrics, Taylor Diagrams were employed to jointly illustrate the correlation coefficient, standard deviation, and RMSE of the models, enabling a comprehensive visual comparison of their predictive abilities. Similarly, Bland–Altman analysis was applied to assess the agreement between measured values and model predictions. This method highlights the mean difference and confidence intervals of the prediction errors, providing further insight into model bias and reliability.

Collectively, these evaluation strategies ensure a robust assessment of prediction accuracy, model stability, and practical usability in piezoelectric energy harvesting applications.

4 Results and Discussion

Although the machine learning algorithms employed in this study (ANN, KNN, SVM, and RF) are well-established and widely used in the literature, their selection was made deliberately in order to ensure a high level of predictive reliability and methodological robustness in impact-driven PVDF-based energy harvesting. The widespread acceptance of these algorithms eliminates uncertainty associated with newly proposed or untested learning architectures and allows the predictive performance to be assessed without algorithm-induced bias.

Rather than focusing on the development of a novel hybrid algorithm, the primary objective of this study was to establish a reliable and physically consistent prediction framework by integrating experimentally derived impact-related parameters with proven machine learning models. The originality of the study therefore lies in the combination of physical energy harvesting behaviour with data-driven prediction, supported by complementary statistical validation tools such as Bland–Altman analysis, Taylor diagrams, and sensitivity assessment.

4.1 Piezo-electric Energy harvesting

Harvesting energy from PVDF materials by periodically applying mechanical stress is a common method. In this study, the same method was used, and periodic impact stress was applied to the PVDF material. To simulate the impact stress, it was rotated using a wheel and pin step motor. The rotation speed was measured with a sensor, and the impact frequency, which is the mechanical stress application frequency, was calculated. The DC output power from the LTC-3588 circuit was measured based on the impact frequency varying between 0 and 6 Hz. A large number of output power measurements have been taken and recorded at different impact frequencies for use in prediction algorithms. In Figure 9, graphs of current, voltage, and power for the electricity generated by the piezoelectric material are provided.

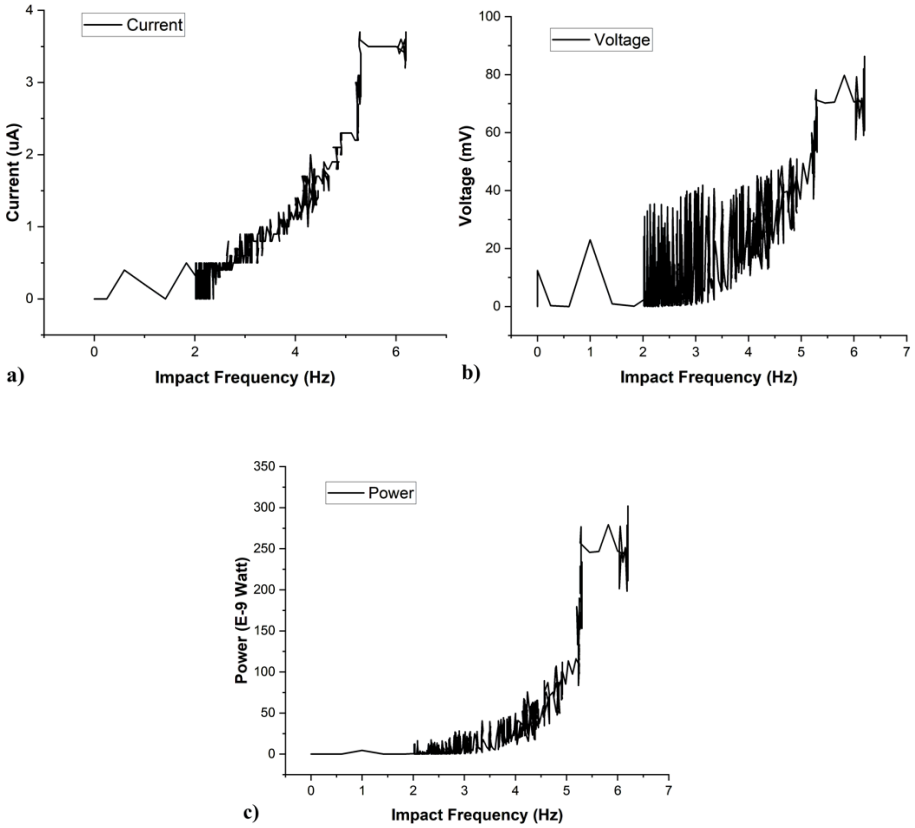

Figure 9: The graphs of current, voltage, and power for the electricity generated by the PVDF

As a result of the experimental study, the maximum output values obtained from the PEH have been determined. As a result of the measurements, the maximum current produced by the system with a 20 K Ohm load resistance was recorded as 3.7 μA, and the voltage as 86.3 mV. The maximum power output corresponding to these values has been calculated as 319.31 nW (approximately 319.31×10−9 Watts). These results indicate that the electrical response of the PVDF-based piezoelectric material to periodic mechanical impacts is measurable but at low power levels. This level of energy has the potential to be used in powering low-power sensors or microelectromechanical systems (MEMS).

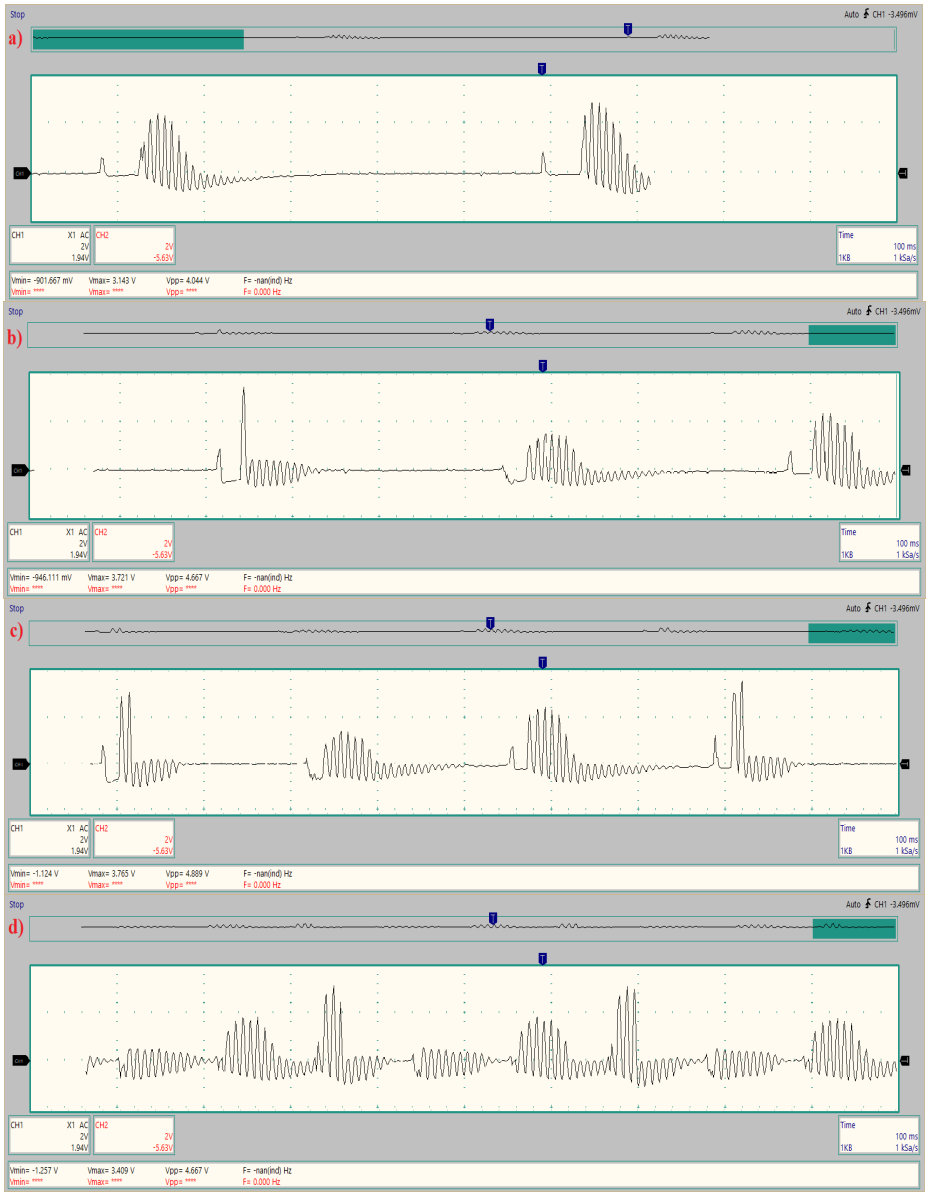

Figure 10: Oscilloscope measurements of the PVDF output at a) 2.0833 Hz, b) 3 Hz, c) 4 Hz and d) 6.1833 Hz

To use the recorded power data in estimation algorithms, an averaging filter must be applied to the data. This is primarily due to the fact that at low pulse frequencies, the mechanical stress within the pulse period ceases, and with the stress cessation, the period during which no voltage is generated within the period lengthens. Because of the lack of voltage generation, both voltage and mechanical stress are recorded as zero

at low pulse frequencies. This can be easily observed in the oscilloscope measurements of the PVDF output at different pulse frequencies shown in Figure 10. Additionally, due to the constant mechanical stress at high pulse frequencies, the voltage does not drop to zero, but all data is filtered to prevent sharp fluctuations. The moving average filter window length is used to filter the voltage outputs at frequency values.

In Figure 10a, the measurement of the PVDF output is shown at a striking frequency of 2.0833 Hz. It is observed that this signal produces power for 200 milliseconds in one period, while no power is generated during the remaining time. The impact frequency in Figures 10b and 10c is 3 Hz and 4 Hz, respectively, while the periods during which the PVDF does not vibrate and the energy production periods are shortened. In Figure 10d, when the impact frequency is 6.1833 Hz, it is observed that there is no period during which energy cannot be generated. For all these reasons, the harvested power data, which form the input to the prediction algorithms, have been regulated with a moving average filter to prevent both the presence and absence of data at the same collision frequency.

4.2 Harvested Energy Prediction

In this study, four different prediction algorithms were used: ANN, KNN, SVM, and RF. The data organized with an average filter were used as input in the models. For the training of the models, 80% of the total data was used, and the remaining 20% was used for testing the models. There are different methods for determining the parameters of the models. In this study, the best results were obtained by selecting parameters according to the type of problem and sometimes using trial-and-error methods. The four different machine learning algorithms used –ANN, KNN, SVM, and RF – were comprehensively evaluated in terms of prediction performance and processing time. According to the metrics in Table 4, although all models showed high accuracy, significant differences in performance levels were observed. Figure 11 shows the Coefficient of Determination (R^2) for the four prediction algorithms. R^2 is a measure of success that indicates how well a regression model explains the data.

Although the R^2 values were relatively close, the key differentiators in the performance assessments of the models were the MAE, RMSE, NSE, and processing time outlined in Table 4. The models demonstrated overall high accuracy; however, they displayed differing degrees of performance regarding error tolerance and computational efficiency. The RF model achieved the highest R^2 value (0.9756), closely followed by the SVM (0.9752) and ANN (0.9730) models, indicating that these approaches explained more than 97% of the variance in the observed data. The KNN model, while still showing strong performance with an R^2 of 0.9464, exhibited comparatively lower generalization ability.

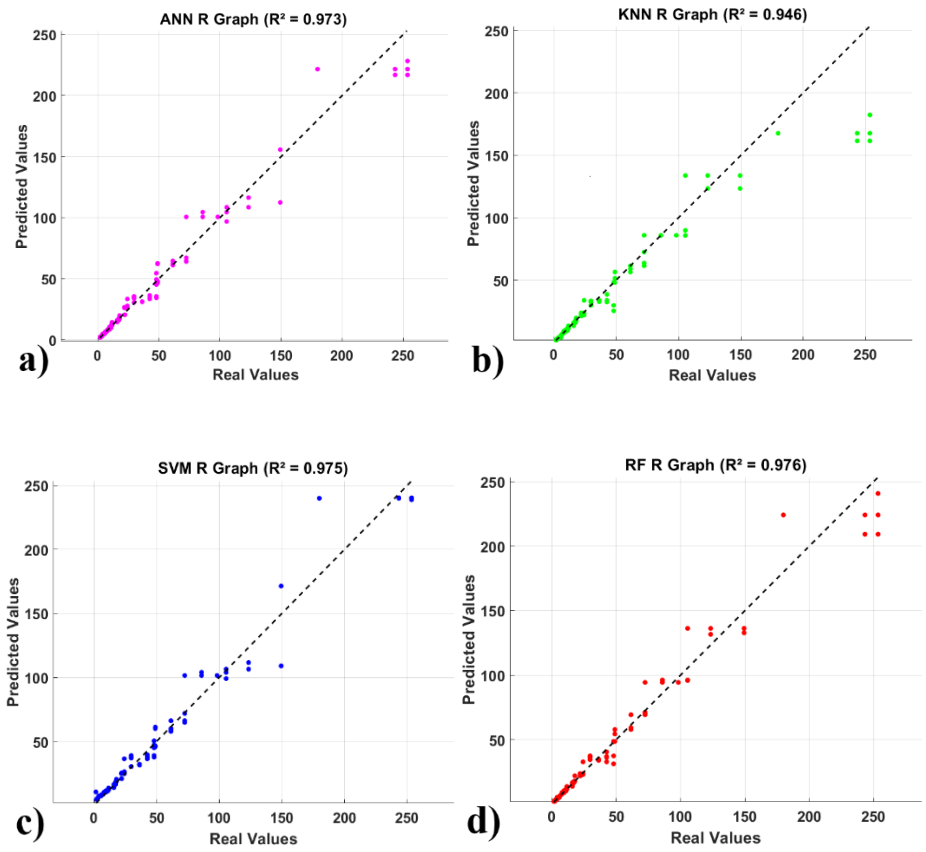

Figure 11: Coefficient of Determination (R^2) of a) ANN, b) KNN, c) SVM and d) RF

Model	R^2	MAE	RMSE	NSE	Processing Time (s)
ANN	0.9730	4.1242	9.3051	0.9715	0.0933
KNN	0.9464	5.2546	16.6871	0.9085	0.0066
SVM	0.9752	4.5296	8.8115	0.9745	0.0230
RF	0.9756	3.5874	8.7020	0.9751	0.0677

Table 4: R^2, MAE, RMSE, NSE, and Processing Time metrics for the models

Upon analysing error measures, specifically MAE and RMSE, the RF model exhibited the lowest error values (MAE = 3.5874, RMSE = 8.7020). This signifies that RF delivers the most reliable and resilient predictive performance among the assessed models. The ANN model demonstrated competitive accuracy, albeit with comparatively greater error magnitudes (MAE = 4.1242, RMSE = 9.3051). The SVM model exhibited performance comparable to RF, with marginally elevated error metrics (MAE = 4.5296, RMSE = 8.8115), whereas the KNN model demonstrated the greatest

error rates (MAE = 5.2546, RMSE = 16.6871), indicating a diminished capacity to accommodate prediction variations.

In terms of the Nash-Sutcliffe Efficiency Coefficient (NSE), the RF model again achieved the highest performance (NSE = 0.9751), followed closely by SVM (0.9745) and ANN (0.9715). The KNN model, on the other hand, showed the lowest NSE value (0.9085), indicating lower reliability in predictive accuracy compared to the other models. Although all models maintained relatively high NSE values, RF and SVM demonstrated stronger efficiency in this dataset.

Regarding processing time, the fastest model was KNN, which completed the prediction process on all test data in only 0.0066 seconds. This speed provides significant advantages in real-time systems. SVM (0.0230 s) and RF (0.0677 s) also offered efficient computational performance, while the ANN model had the longest processing duration (0.0933 s), which may be attributed to the iterative and parameter-intensive nature of neural network training.

In conclusion, the RF model stands out as the most balanced and successful approach, combining high accuracy (R^2 = 0.9756), low error rates, and efficient processing time. The SVM model also performed competitively, offering both high accuracy and stability. While the ANN model provides high predictive success, its relatively longer computation time may be a limitation for time-critical applications. Conversely, the KNN model, despite being the fastest, showed weaker predictive performance and higher error values, limiting its applicability in scenarios requiring precise accuracy.

In Figure 12, the comparison of the predicted values produced by the four developed machine learning models – ANN, KNN, SVM, and RF – with the actual (target) values is visually presented. On the horizontal axis, the sample number (Sample) is represented, while the actual/predicted values (Target / Prediction) are shown on the vertical axis. Each model is represented by a different colour and line style, providing a clear comparative visualization of their performances.

In addition to the common error metrics, the Artificial Neural Network (ANN) model was also evaluated in terms of training and testing errors. The obtained results (MSEtrain = 139.76 vs. MSEtest = 86.59) indicate that the model was able to generalize the dataset effectively without significant overfitting. The relatively close values of training and testing errors confirm that the ANN model has achieved a balance between learning capacity and prediction ability, although slightly higher training error suggests that the network avoided memorization and maintained generalization performance.

Overall, it is observed that the prediction curves of all models largely overlap with the black-coloured "real" data curve, indicating that the models achieved relatively high accuracy during the learning process and were able to generalize the data to a considerable extent. The region after the 200th sample, where the system output shows a sudden increase, serves as a critical range to test the accuracy of the models. In this region, the RF and SVM models showed the closest alignment with the real data, while the ANN model followed the curve with slightly higher error values. In contrast, the KNN model exhibited larger deviations, particularly in sharp transitions.

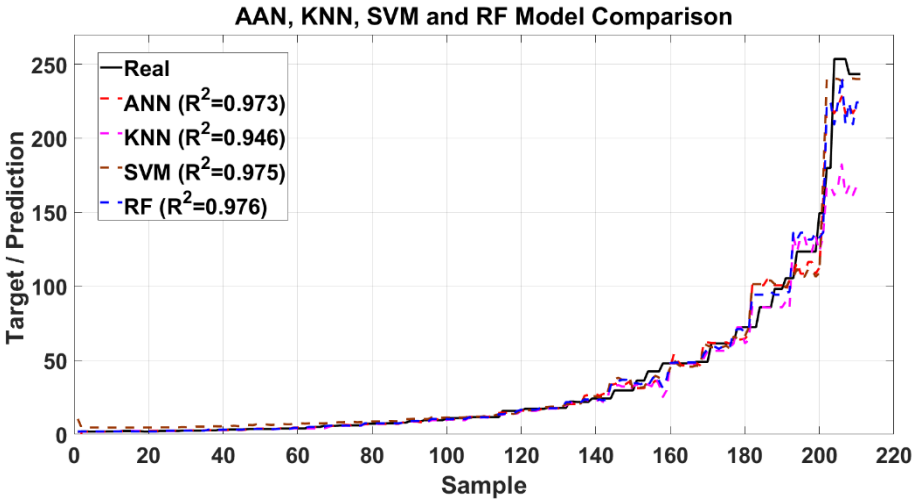

Figure 12: The comparative graph of the prediction results of the developed ANN, KNN, SVM, and RF models with the actual (target) values

The RF model demonstrated the most stable prediction performance, aligning closely with the real curve in both sudden increases and low-amplitude regions, consistent with its strong performance metrics (R^2 = 0.9756, MAE = 3.5874, RMSE = 8.7020, NSE = 0.9751). Similarly, the SVM model performed robustly (R^2 = 0.9752, NSE = 0.9745), though minor fluctuations were noted during steep transitions. The ANN model, despite producing accurate predictions overall (R^2 = 0.9730), showed slightly higher deviations in nonlinear ranges, which indicates that its learning capacity may be somewhat limited in capturing complex transitions. The KNN model, while being the fastest in computation (0.0066 s), displayed the weakest alignment with the real curve (R^2 = 0.9464, RMSE = 16.6871, NSE = 0.9085), especially in sudden increase regions, suggesting reduced robustness compared to the other models.

The superior performance of the RF and SVM models compared to ANN and KNN can be directly related to the nonlinear and nonstationary electromechanical behaviour of PVDF materials under impact excitation. Impact-driven piezoelectric responses inherently involve abrupt transitions, transient dynamics, and measurement noise. The kernel-based structure of SVM enables the effective mapping of such nonlinear input–output relationships into a high-dimensional feature space, providing strong generalization capability even for relatively small datasets.

Likewise, the ensemble learning nature of RF inherently enhances robustness against noise and sudden signal variations by averaging multiple independent regression trees. This property is particularly advantageous for impact-induced piezoelectric signals, where sharp voltage peaks and intermittent zero-crossings are commonly observed. The superior accuracy achieved by the RF model aligns with the nonlinear strain–charge dynamics inherent to piezoelectric materials, particularly under periodic impact conditions where deformation amplitude and charge generation vary sharply with frequency. Ensemble-based methods such as RF are well suited to

capturing these irregularities, which explains their stronger resilience across both low- and high-amplitude regions. In contrast, ANN performance may be sensitive to local minima and initial weight distributions under limited data conditions, while KNN is strongly affected by local data sparsity and noise contamination. The behaviour of the ANN model, characterised by a higher training error relative to testing error, suggests that the network benefited from an implicit form of regularization, likely influenced by the uneven distribution of data across frequency ranges and the network's ability to smooth local fluctuations rather than memorise them. Furthermore, beyond predictive accuracy, the practical implications of the developed models are notable. The prediction outputs generated by these algorithms may be integrated into real-time control strategies, such as adaptive load matching, dynamic tuning of excitation frequency, or automated adjustment of cantilever–impact configurations. These applications highlight how data-driven modelling can support the optimisation of piezoelectric energy harvesters by linking statistical predictions with the physical mechanisms governing energy conversion.

Despite the promising predictive performance obtained in this study, several limitations must be acknowledged. First, the experimental investigation was conducted using a single type of PVDF material, which may restrict the generalizability of the obtained models to other piezoelectric composites or multilayer structures. Second, the impact excitation was applied within a limited frequency range under controlled laboratory conditions. Finally, although 1058 samples provide a meaningful basis for model comparison, the dataset size remains relatively small for broader deep-learning generalization.

Future research will focus on extending the proposed prediction framework to multi-axis vibration conditions, incorporating different piezoelectric materials (such as PZT and composite laminates), and implementing real-time embedded prediction systems for autonomous energy harvesting applications. These extensions are expected to significantly enhance both the physical applicability and technological impact of the proposed methodology.

4.3 Statistical Agreement of Models

In addition to conventional error metrics (R^2, MAE, RMSE, NSE), advanced statistical techniques such as the Taylor diagram and Bland-Altman analysis were employed to further investigate the agreement and reliability of the developed models.

The results obtained in this study show that all models performed with high overall accuracy. When examining the Taylor diagram provided in Figure 13, it is observed that the RF (Random Forest) and SVM (Support Vector Machine) models have the highest correlation with the observations ($R \approx 0.975$) and the closest standard deviation values to the observations. This situation reveals that both models are more successful in capturing changes in system output in terms of amplitude and phase alignment. The ANN (Artificial Neural Network) model also provided a high correlation coefficient ($R^2 = 0.9730$) and exhibited strong performance in terms of overall accuracy; however, when error metrics were evaluated, it had higher RMSE (9.3051) and MAE (4.1242) values compared to RF and SVM. The KNN (K-Nearest Neighbour) model, on the other hand, stands out with lower correlation ($R^2 = 0.9464$) and higher error values (RMSE = 16.6871, MAE = 5.2546) compared to the other models.

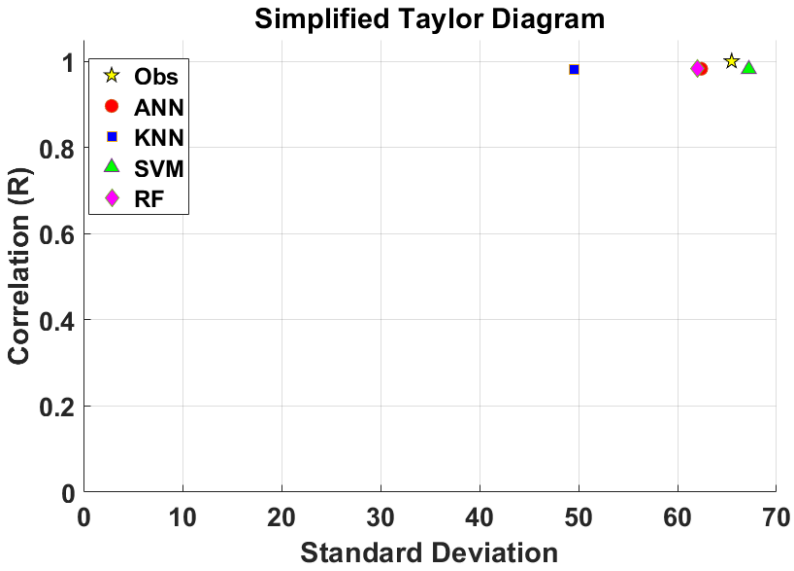

Figure 13: Simplified Taylor diagram comparison of models

The simultaneous evaluation of numerical metrics and the Taylor diagram revealed that the RF and SVM models demonstrated the most effective and balanced performance, the ANN model yielded satisfactory accuracy, whereas the KNN model underperformed relative to the others due to elevated error rates, notwithstanding its benefits of simplicity and minimal processing time.

The Bland-Altman plot given in Figure 14 shows the distribution of differences between observed and predicted values relative to the mean. The mean bias line is positioned very close to zero, indicating that all models have a low level of systematic bias.

The point distributions of the RF and ANN models are largely clustered within a ±20 error band. This situation reveals that both models exhibit high accuracy and low variance in their predictions. The SVM model also resulted in low bias, but showed a wider distribution, especially in the region of high average values. KNN models, on the other hand, exhibited a more heterogeneous distribution compared to other models; deviations exceeding ±50 was observed, particularly at average values above 150. This finding indicates that the KNN model produces fewer stable results, especially in regions with high-amplitude outputs.

Overall, the Bland-Altman analysis reveals that the prediction performance of the RF and ANN models is more balanced and reliable, SVM exhibits an acceptable level of accuracy, and KNN is limited in terms of accuracy despite its simplicity and speed advantage. This analysis emphasizes that error distributions must be considered not only with average performance metrics but also with the systematic trends of prediction deviations.

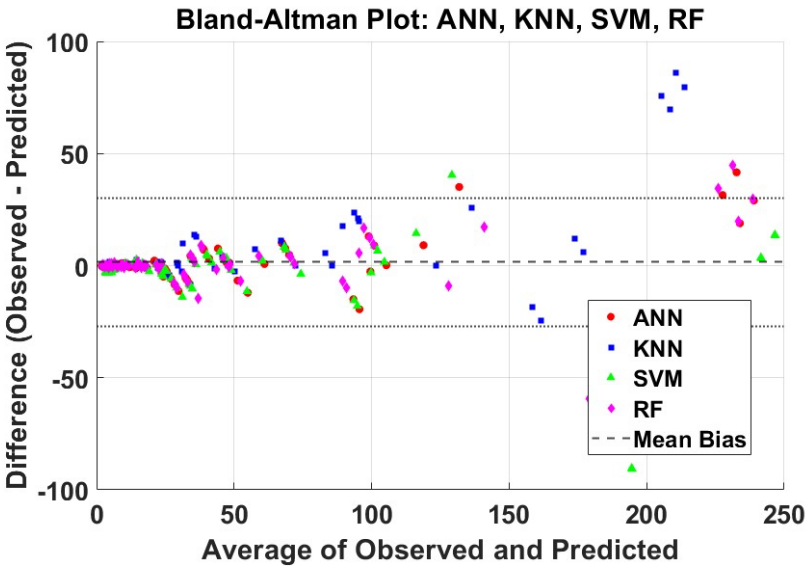

Figure 14: Bland-Altman plot of models

5 Conclusions

In this study, an experimental setup was prepared to measure the energy that can be harvested depending on the periodic mechanical impact frequency using PVDF piezoelectric material. Based on the data obtained from the experimental setup, prediction models were developed using ANN, KNN, SVM, and RF algorithms. The models were compared in terms of statistical performance metrics (R^2, MAE, RMSE, NSE) as well as computational time.

The analysis results demonstrated that all models achieved high accuracy, with R^2 values ranging between 0.9464 and 0.9756. The lowest error rates were observed in the RF model, followed closely by the SVM model. Although the ANN model also showed competitive performance, its error magnitudes were slightly higher compared to RF and SVM. The KNN model, despite its lower accuracy, exhibited the shortest processing time, making it a strong candidate for real-time applications.

Beyond conventional performance metrics, Taylor diagram analysis confirmed that RF and SVM were positioned closest to the observation point, reflecting their superior ability to capture both correlation and variance characteristics of the data. Meanwhile, Bland-Altman analysis revealed that RF and ANN predictions clustered tightly around the zero-bias line, indicating low systematic errors, while KNN predictions showed larger deviations, particularly in high-amplitude regions. These complementary analyses strengthen the conclusion that RF and SVM provide the most balanced performance, while KNN offers a practical alternative for fast, real-time scenarios.

In conclusion, for nonlinear and complex systems such as piezoelectric energy harvesting, data-driven approaches deliver reliable and effective results. Among the models evaluated, the RF and SVM algorithms stand out as the most accurate and

consistent, while KNN is particularly attractive for applications requiring rapid predictions. The prediction models developed in this study provide valuable guidance for researchers focusing on energy harvesting systems driven by periodic impact stresses.

Future studies will focus on the development of hybrid machine learning architectures, such as RF–ANN or neuro-fuzzy models, to further enhance prediction accuracy under complex impact excitation conditions.

References

[Ahmad and Allard, 2011] Ahmad, F. M., and Allard, M. J. M. (2011). Agricultural drought forecasting using satellite images, climate indices and artificial neural network. International Journal of Remote Sensing, 32(24), 9707–9719. doi:10.1080/01431161.2011.575896

[Aga et al., 2020] Aga, M., Teuku, R. N., Rinaldi, I., Novi, R. S., Rivansyah, S., and Irvanizam, I. (2020). Prediction of Kovats Retention Indices for Fragrance and Flavor using Artificial Neural Network, In Proc. 2020 International Conference on Electrical Engineering and Informatics (ICELTICs), IEEE, pages 1–5. doi:10.1109/ICELTICs50595.2020.9315391

[Amin et al., 2025] Amin, M., Javad, H., and Victor, C. M. L. (2025). Dynamic Offloading in Mobile Edge Computing with Traffic-Aware Network Slicing and Adaptive TD3 Strategy. IEEE Communications Letters, 29(1), 95–99. doi:10.1109/LCOMM.2024.3501956

[Baozhi et al., 2021] Baozhi, W., Chenggong, Z., Liyan, L., Xuan, D., and Yigui, L. (2021). Design, Manufacture and Test of Piezoelectric Cantilever-Beam Energy Harvesters with Hollow Structures. Micromachines, 12(9), 1090. doi:10.3390/mi12091090

[Bin et al., 2022] Bin, Z., Hongsheng, L., Shengxi, Z., and Jun, G. (2022). A review of nonlinear piezoelectric energy harvesting interface circuits in discrete components. Applied Mathematics and Mechanics, 43(7), 1001–1026. doi:10.1007/s10483-022-2863-6

[Bishal et al., 2024] Bishal, P., Dewasis, D., Mandip, B., and Ajay, K. (2024). Assessing Meteorological Drought Patterns and Forecasting Accuracy with SPI and SPEI Using Machine Learning Models. Forecasting, 6(4), 1026–1044. doi:10.3390/forecast6040051

[Cevat et al., 2021] Cevat, V. K., Seyda, E., Nezih, T., and A. Fethi O. (2021). Optimization of beam profiles for improved piezoelectric energy harvesting efficiency. Structural and Multidisciplinary Optimization, 63(2), 631–643. doi:10.1007/s00158-020-02714-0

[Chengliang Sun et al., 2009] Chengliang, S., Lifeng, Q., Fang, L., and Qing-Ming, W. (2009). Piezoelectric Energy Harvesting using Single Crystal Pb(Mg1/3Nb2/3)O 3-xPbTiO3 (PMN-PT) Device. Journal of Intelligent Material Systems and Structures, 20(5), 559–568. doi:10.1177/1045389x08097385

[Chengyun et al., 2021] Chengyun, Z., Gang, H., Daniil, Y., Pengfei, L., Shanghao, G., Dongran, S., Huayi, P., and Junlei, W. (2021). Machine learning based prediction of piezoelectric energy harvesting from wake galloping. Mechanical Systems and Signal Processing, 160, 107876. doi:10.1016/j.ymssp.2021.107876

[Corinna and Vladimir, 1995] Corinna, C., and Vladimir, V. (1995). Support-vector networks. Machine Learning, 20(3), 273–297. doi:10.1007/BF00994018

[Domenico et al., 2022] Domenico, T., Federico, M., Bruno, B., Thibault, D. L. W., Enrique, D. P. C., and Alberto, D. (2022). Vibration Energy Harvesting by Means of Piezoelectric Patches: Application to Aircrafts. Sensors, 22(1), 363. doi:10.3390/s22010363

[Ernest et al., 2020] Ernest, Y. B., Joseph, O., and Daniel, A. A. (2020). Basic Tenets of Classification Algorithms K-Nearest-Neighbor, Support Vector Machine, Random Forest and Neural Network: A Review. Journal of Data Analysis and Information Processing, 08(04), 341–357. doi:10.4236/jdaip.2020.84020

[Faizan et al., 2019] Faizan, A., Waseem, R., Xilin, L., Hajera, G., and Ki-Hyun, K. (2019). Piezoelectric energy harvesters for biomedical applications. Nano Energy, 57, 879–902. doi:10.1016/j.nanoen.2019.01.012

[Fei et al., 2004] Fei, P., Baoying, W., Xin, H., and William, P. (2004). Comprehensive vertical sample-based KNN/LSVM classification for gene expression analysis. Journal of Biomedical Informatics, 37(4), 240–248. doi:10.1016/j.jbi.2004.07.003

[Hao et al., 2013] Hao, W., Lihua, T., Yaowen, Y., and Chee, K. S. (2013). A novel two-degrees-of-freedom piezoelectric energy harvester. Journal of Intelligent Material Systems and Structures, 24(3), 357–368. doi:10.1177/1045389X12457254

[Harvey et al., 2022] Harvey, N. C., Ahmed, M. R. F. E., Bernard, W. I., and Evan, M. (2022). Development of a varying multi-cantilever beam frequency up conversion energy harvester. Energy Conversion and Management: X, 16, 100290. doi:10.1016/j.ecmx.2022.100290

[Henry et al., 2004] Henry, A. S., Daniel, J. I., and Gyuhae, P. (2004). A Review of Power Harvesting from Vibration Using Piezoelectric Materials. The Shock and Vibration Digest, 36(3), 197–205. doi:10.1177/0583102404043275

[Huicong et al., 2018] Huicong, L., Junwen, Z., Chengkuo, L., Seung-Wuk, L., and Liwei, L. (2018). A comprehensive review on piezoelectric energy harvesting technology: Materials, mechanisms, and applications. Applied Physics Reviews, 5(4), 041306. doi:10.1063/1.5074184

[Ismail et al., 2008] Ismail, H., Bilal, H., and Eyas, E. (2008). Performance of KNN and SVM classifiers on full word Arabic articles. Advanced Engineering Informatics, 22(1), 106–111. doi:10.1016/j.aei.2007.12.001

[Irvanizam et al., 2023] Irvanizam, I., Ivan, H., and Hizir, S. (2023). Applying Artificial Neural Network Based on Backpropagation Method for Indonesian Sign Language Recognition. International Journal of Computing and Digital Systems, 14(1), 975–985. doi:10.12785/ijcds/140176

[Jaime et al., 2019] Jaime, L. S., Michael, E. M., Janet, T., and Edward, I. (2019). A comparison of random forest variable selection methods for classification prediction modeling. Expert Systems with Applications, 134, 93–101. doi:10.1016/j.eswa.2019.05.028

[Jie et al., 2018] Jie, Z., Xushi, N., Xiaojuan, H., Jian, H., Xiujian, C., Chenyang, X., and Wendong, Z. (2018). Highly Reliable Real-time Self-powered Vibration Sensor Based on a Piezoelectric Nanogenerator. Energy Technology, 6(4), 781–789. doi:10.1002/ente.201700614

[Kurt et al., 1990] Kurt, H., Maxwell, S., and Halbert, W. (1990). Universal approximation of an unknown mapping and its derivatives using multilayer feedforward networks. Neural Networks, 3(5), 551–560. doi:10.1016/0893-6080(90)90005-6

[Leo, 1996] Leo, B. (1996). Bagging predictors. Machine Learning, 24(2), 123–140. doi:10.1007/BF00058655

[Linbing et al., 2019] Linbing, W., Xinlong, T., Hailu, Y., Ya, W., and Yinghao, M. (2019). Design and analysis of a hollow triangular piezoelectric cantilever beam harvester for vibration energy collection. International Journal of Pavement Research and Technology, 12(3), 259–268. doi:10.1007/s42947-019-0032-1

[Mahyar et al., 2019] Mahyar, S., Kamyar, S., Mohammad, M. A., Majid, F., Vahid, Z. B., Hangyue, L., Mischa, D., and Minoo, N. (2019). Towards a Green and Self-Powered Internet of Things Using Piezoelectric Energy Harvesting. IEEE Access, 7, 94533–94556. doi:10.1109/ACCESS.2019.2928523

[Mariza et al., 2022] Mariza, A., Teuku, R. N., Aga, M., Rivansyah, S., Muslem, M., Novi, R. S., Ghazi, M. I., Souvia, R., Razief, P. F. A., Muhammad, S., Irvanizam, I., and Rinaldi, I. (2022). Application of Fuzzy Support Vector Regression to Predict the Kovats Retention Indices of Flavors and Fragrances, In Proc. 2022 International Conference on Electrical Engineering and Informatics (ICELTICs), IEEE, pages 13–18. doi:10.1109/ICELTICs56128.2022.9932124

[Measurement Specialties, 1999] Measurement Specialties (1999). Piezo Film Sensors Technical Manual. www.msiusa.com

[Mikko et al., 2016] Mikko, L., Jari, J., Heli, J., and Jaakko, P. (2016). Energy Harvesting with a Bimorph Type Piezoelectric Diaphragm Multilayer Structure and Mechanically Induced Pre-stress. Energy Technology, 4(5), 620–624. doi:10.1002/ente.201500429

[Prabina et al., 2016] Prabina, K. M., Tanmaya, K. S., and A. R. R. (2016). Performance evaluation of neural network, support vector machine and random forest for prediction of donor splice sites in rice. Indian Journal of Genetics and Plant Breeding (The), 76(2), 173. doi:10.5958/0975-6906.2016.00027.4

[Priyadarshini et al., 2017] Priyadarshini, P., Nagaratna, Y., and S.M. M. (2017). Comparision of Performance of Classifiers - SVM, RF and ANN in Potato Blight Disease Detection Using Leaf Images, In Proc. 2017 IEEE International Conference on Computational Intelligence and Computing Research (ICCIC), IEEE, pages 1–5. doi:10.1109/ICCIC.2017.8524301

[Qinghua et al., 2025] Qinghua, S., Junru, Y., and Amin, M. (2025). Multi-Objective Resource Optimization in UAV-Enabled Heterogeneous Cellular Networks Using Serverless Federated Learning and Power-Domain NOMA. Transactions on Emerging Telecommunications Technologies, 36(8), e70210. doi:10.1002/ett.70210

[Robert et al., 2007] Robert, E. B., Lawrence, O. H., Kevin, W. B., and W. P. K. (2007). A Comparison of Decision Tree Ensemble Creation Techniques. IEEE Transactions on Pattern Analysis and Machine Intelligence, 29(1), 173–180. doi:10.1109/TPAMI.2007.250609

[Serkan and Burcu, 2024] Serkan, K., and Burcu, Ö. B. (2024). Tourism Demand Forecasting with Support Vector Regression, Ridge Regression, And Multiple Linear Regression Methods. Journal of Research in Business, 9(1), 194–218. doi:10.54452/jrb.1395182

[Shashank et al., 2019] Shashank, P., Hyun-Cheol, S., Yuan, Z., Ronnie, V., Anuj, C., Sang-Gook, K., Isaku, K., Liao, W., Dong, S. H., Jungho, R., and Ronald, G. P. (2019). A Review on Piezoelectric Energy Harvesting: Materials, Methods, and Circuits. Energy Harvesting and Systems, 4(1), 3–39. doi:10.1515/ehs-2016-0028

[Shashank et al., 2009] Shashank, P., Kim, H., and Tadesse, Y. (2009). Energy Harvesting Technologies. Springer US, Boston, MA. doi:10.1007/978-0-387-76464-1

[Shima et al., 2018] Shima, S., Sihong, Z., and Alper, E. (2018). Soft and Hard Piezoelectric Ceramics and Single Crystals for Random Vibration Energy Harvesting. Energy Technology, 6(5), 935–942. doi:10.1002/ente.201700873

[Shuhong et al., 2024] Shuhong, K., Jiyong, Z., and Amin, M. (2024). Reliable information delivery and dynamic link utilization in MANET cloud using deep reinforcement learning. Transactions on Emerging Telecommunications Technologies, 35(9), e5028. doi:10.1002/ett.5028

[Sung et al., 2019] Sung, S., W., Hosung, S., Masami, K., Sebastjan, G., Jinkee, L., Yunseok, K., Chang, K. J., Angus, I. K., and Seung-Hyun, K. (2019). Flexible vibrational energy harvesting devices using strain-engineered perovskite piezoelectric thin films. Nano Energy, 55, 182–192. doi:10.1016/j.nanoen.2018.10.068

[Suykens and Vandewalle, 1999] J A K Suykens, and J Vandewalle. (1999). Least Squares Support Vector Machine Classifiers. Neural Processing Letters. Neural Processing Letters 9, 293–300

[Tarun et al., 2015] Tarun, K., Rajeev, K., Vishal, S. C., and Jens, T. (2015). Finite-Element Analysis of a Varying-Width Bistable Piezoelectric Energy Harvester. Energy Technology, 3(12), 1243–1249. doi:10.1002/ente.201500191

[Teuku et al., 2022] Teuku, R. N., Aga, M., Novi, R. S., Rivansyah, S., Irvanizam, I., Ghazi, M. I., Muhammad, Y., Taufik, F. A., and Rinaldi, I. (2022). The Prediction of Kovats Retention Indices of Essential Oils at Gas Chromatography Using Genetic Algorithm-Multiple Linear Regression and Support Vector Regression. Journal of Engineering Science and Technology, 17(1), 0306-0326.

[Thomas, 2000] Thomas, G. D. (2000). An Experimental Comparison of Three Methods for Constructing Ensembles of Decision Trees: Bagging, Boosting, and Randomization. Machine Learning, 40, 139–157

[Umit et al., 2021] Ümit, A., Ali, E. G., and Yunus, B. (2021). Prediction of daily global solar radiation using different machine learning algorithms: Evaluation and comparison. Renewable and Sustainable Energy Reviews, 135, 110114. doi:10.1016/j.rser.2020.110114

[Wael et al., 2022] Wael, A., Lea, Č., and Andrej, Š. (2022). Hydrological Drought Forecasting Using Machine Learning—Gidra River Case Study. Water, 14(3), 387. doi:10.3390/w14030387

[Yuzhong et al., 2020] Yuzhong, X., Fang, S., and Xinghuan, L. (2020). A piezoelectric cantilever-beam energy harvester (PCEH) with a rectangular hole in the metal substrate. Microsystem Technologies, 26(3), 801–810. doi:10.1007/s00542-019-04608-8